Published in final edited form as:
J Neural Eng. 2014 February ; 11(1): 016010. doi:10.1088/1741-2560/11/1/016010.

Optogenetic micro-electrocorticography for modulating and localizing cerebral cortex activity

Thomas J. Richner[1,6], **Sanitta Thongpang**[1,2,6], **Sarah K. Brodnick**[1], **Amelia A. Schendel**[3], **Ryan W. Falk**[4], **Lisa A. Krugner-Higby**[5], **Ramin Pashaie**[4], and **Justin C. Williams**[1,3]
Thomas J. Richner: richner@wisc.edu

[1]Biomedical Engineering, University of Wisconsin-Madison, Madison, WI, USA [2]Biomedical Engineering, Mahidol University, Salaya, Nakornpathom, Thailand [3]Material Science, University of Wisconsin-Madison, Madison, WI, USA [4]Electrical Engineering and Computer Science, University of Wisconsin-Milwaukee, Milwaukee, WI, USA [5]Surgical Sciences, School of Veterinary Medicine, University of Wisconsin-Madison, Madison, WI, USA

Abstract

Objective—Spatial localization of neural activity from within the brain with electrocorticography (ECoG) and electroencephalography (EEG) remains a challenge in clinical and research settings, and while microfabricated ECoG (micro-ECoG) array technology continues to improve, complimentary methods to simultaneously modulate cortical activity while recording are needed.

Approach—We developed a neural interface utilizing optogenetics, cranial windowing, and micro-ECoG arrays fabricated on a transparent polymer. This approach enabled us to directly modulate neural activity at known locations around micro-ECoG arrays in mice expressing Channelrhodopsin-2 (ChR2). We applied photostimuli varying in time, space and frequency to the cortical surface, and we targeted multiple depths within the cortex using an optical fiber while recording micro-ECoG signals.

Main Results—Negative potentials of up to 1.5 mV were evoked by photostimuli applied to the entire cortical window, while focally applied photostimuli evoked spatially localized micro-ECoG potentials. Two simultaneously applied focal stimuli could be separated, depending on the distance between them. Photostimuli applied within the cortex with an optical fiber evoked more complex micro-ECoG potentials with multiple positive and negative peaks whose relative amplitudes depended on the depth of the fiber.

Significance—Optogenetic ECoG has potential applications in the study of epilepsy, cortical dynamics, and neuroprostheses.

1. Introduction

Recording potentials from the surface of the brain, electrocorticography (ECoG), was originally developed to functionally map the cerebral cortex in patients with epilepsy [1].

[6]These authors contributed equally.

More recently, brain-computer interfaces (BCIs) have been implemented based on ECoG [2,3]. Both epilepsy and BCI applications of ECoG could benefit from improved interface technology. High density microfabricated ECoG (micro-ECoG) arrays have been developed to record from large cortical areas at high resolution [4,5], and chronically implanted micro-ECoG arrays show promise for BCI applications [6]. While recording devices continue to improve, complementary approaches to simultaneously stimulate cortical activity would be useful for many applications. Such bidirectional cortical interfaces could be used to study the dynamics of epilepsy, to validate inverse models that relate potentials measured on the surface of the cortex to localized neural activity at known locations, or to create BCIs with sensory feedback.

Electrical microstimulation and transcranial magnetic stimulation (TMS) are potential methods that could be combined with ECoG to implement a bidirectional interface. Microstimulation is used to excite small volumes of neurons [7], but simultaneous recording can be difficult due to potential electrical artifacts. Custom electrical hardware can significantly reduce artifact size [8], but artifacts cannot be completely avoided. Artifacts are also created by TMS, and while TMS has the benefit of being non-invasive, it has relatively low spatial resolution and limited ability to stimulate at multiple locations simultaneously.

Optogenetics is potentially an ideal technology to be combined with micro-ECoG electrode arrays to create a bidirectional neural interface. Optogenetics is an emergent field that offers the ability to excite or inhibit a specific neuron type with light sensitive ion channels or pumps [9–11]. Since optogenetics leverages the inherent properties of modern optical systems, it can be used on a similar spatial resolution as electrode arrays and can modulate multiple locations simultaneously. Researchers have previously combined optogenetic modulation with neural electrode recording technologies, primarily through the integration of optical fibers with silicon or wire intracortical electrodes [12–16]. Optically induced recording artifacts are a potential problem [17], and even though the high work function of the noble metals can help prevent the photoelectric effect, the Becquerel effect is still a concern [18]. Carefully designing the device to minimize the amount of light incident on the exposed sites can help prevent this problem. Optical waveguides or LED arrays [19] have been used as light delivery technologies and could be integrated into micro-ECoG electrodes, although high density optical connections are challenging to fabricate, and photostimulation would be limited to a finite set of locations.

Alternatively, cranial windowing, a surgical technique in which the skull is replaced with a small piece of cover glass [20,21], could also be adapted for optogenetic photostimulation and electrode implantation. Cranial windowing is most often used for optical imaging of the cortex [22], but it has also been used to deliver optogenetic stimulation [12,22,23]. The depth of optical penetration through the cortex is limited [23–25], but focused or collimated light, in comparison to light diverging from an optical fiber, could be used to stimulate at greater depths. Cranial windowing could be further adapted for implantation of thin devices such as micro-ECoG arrays.

In this study, we developed an optogenetic micro-ECoG platform by implanting a custom thin-film electrode array under a cranial window in an optogenetic mouse model. Utilizing

both LEDs and a fiber-coupled laser, we investigated the spatial, temporal, and spectral properties of the optogenetic micro-ECoG platform. We investigated the spatial separation of multiple optical sources, the evoked waveform of optogenetic stimulation at different depths within the cortex, and the response of the cortex to complex stimuli that vary in space, time, and frequency.

2. Methods

Our approach integrates electrode arrays microfabricated on a transparent polymer, windowing techniques adapted from *in vivo* imaging, and optogenetics to create a bidirectional chronic neural interface in mice. We fabricated custom micro-scale ECoG (micro-ECoG) electrode arrays on Parylene C (figure 1(b)) using a lift-off photolithography process (figure 1(a)). We implanted Parlyene C based arrays under a cranial window (figure 1(d)) in Thy1::Channelrhodopsin-2/H134R (ChR2) mice (5 mice chronic implantation, 5 mice acute, 2 wild type mice for control). Blood vessels were clearly visible through the array and cranial window up to 6 weeks after implantation (figure 1(e)). The platinum electrode sites and connecting traces occluded only 8.3% of the array's area, so the cortex could be readily modulated by photostimuli applied through the window and array.

2.1. Electrode fabrication

Custom micro-ECoG electrodes were fabricated by patterning platinum electrode sites on a transparent insulative substrate polymer, Parylene C. This transparent substrate was chosen so that photostimuli could be applied through the array and onto the cortex. In comparison, polyimide, another material commonly used in flexible electrode arrays, blocks blue light considerably (supplementary figure 1). Parylene C is a biocompatible polymer for neural implants [26,27] that has been used as an insulator for microwire electrodes [28,29] and more recently as a substrate for flexible electrode arrays [30]. We fabricated our thin film micro-ECoG arrays with a biocompatible lift-off process including chemical vapor deposition, photolithography, and plasma etching (figure 1(a)). First, we deposited a layer of Parylene 15 μm thick on a silicon wafer. Second, we patterned metal layers (10 nm Cr, 200 nm Au, and 20 nm Pt) using photolithography and lift-off to form the electrical connection traces and electrode sites. Alternatively, a transparent metal layers such as indium tin oxide could be used for more transparent arrays [31]. The sites (150 μm in diameter) were arranged in a 4x4 grid with 500 μm site-to-site spacing. Next, we deposited a 10 μm layer of Parylene and etched with oxygen plasma (790, Unaxis) to expose the platinum electrode sites. We spun two 24 μm layers of AZ P4620 photoresist (AZ Electronic Materials) on as a mask during oxygen plasma etching. We chose oxygen plasma over more aggressive etching processes to preserve biocompatibility. Last, we released the arrays from the silicon wafer in a water bath.

Once the arrays were separated from the wafer, we bolstered the connector pad region with a polyimide backing to add the thickness required (200 μm) by the flexible printed circuit connector. We cut these backings out of 175 μm polyimide sheet (Pryalux LF, Dupont) with a cutting plotter (CE5000-40-CRP, Graphtec), and bonded them to the electrode pad area with the adhesive included on the polyimide sheet at 180° C and 235 kPa for 1 hour.

We inserted Parylene electrodes with polyimide connector backings into custom printed circuit boards (PCBs) to finish assembly (figure 1(c)). We designed the boards with Eagle (CadSoft) and had the boards fabricated and assembled (Imagineering Inc.) with surface mounted connectors. A flexible printed circuit connector (FH26, Hirose) accepts the electrodes, and the PCB routes the signals to a zero insertion force connector (DF30, Hirose) compatible with Tucker-Davis Technology amplifiers. We chose this mechanical connection scheme due to the difficulty of soldering platinum and to speed the assembly process. Once assembled, we measured the electrical impedance spectrum [32] (PGSTAT 128N, Metrohm) of the arrays in a dish of Saline to ensure typical values (e.g. 50 kOhms @ 1 kHz) at every site prior to implantation.

2.2. Cranial window implantation

We obtained Thy1::ChR2/H134R-YFP mice, one of the many optogenetic strains created by Guoping Feng [33,34], from the Jackson Laboratory (stock number 012350) and bred these hemizygous mice to wild type (WT) females to maintain a breeding colony. We chose mice with the H134R point mutation of ChR2 to reduce the intensity of light required to achieve photostimulation, but at the expense of slower channel kinetics [35–37].

In vivo experiments were approved by the Institutional Animal Care and Use Committee at the University of Wisconsin-Madison. The cranial windowing method has been used for many decades [20], and multiple investigators have adapted and improved the approach for specific applications [22,38–42]. Our approach adds implantation of a flexible array epidurally, underneath the cranial window (figure 1(d) and (e)) [43]. Dexamethasone (1 mg/kg SC) was administered on the day prior to surgery and again on the day of surgery to prevent cerebral edema. Buprenorphine (0.05 mg/kg SC) and ampicillin (100 mg/kg SC) were given 30 minutes before surgery, and glycopyrolate (0.02 mg/kg SC) was administered as the procedure began. Sterile implantation surgery was done in isoflurane-anesthetized mice (1.5–2.0% in oxygen).

The mouse was shaved, mounted in a mouse stereotaxic frame (Cunningham Mouse Adapter, Leica), and the surgical site was cleaned. An incision was made over the calvarium to expose the bregma and lambda sutures, and the connective tissue was removed with cotton swabs. UV acrylic (Fusio, Pentron) was applied in front of bregma, behind lamba, and around the periphery of exposed bone. Bone screws were not used due to the limited bone thickness, so the ground/ref wire was coiled and implanted over an area of thinned skull, similar to that used for thinned skull *in vivo* imaging, on the side contralateral to the cranial window. The bone was thin enough, and the area of the coiled wire was sufficient, to provide a low impedance ground connection. A drill (Micromotor Drill, Leica) was used with a burr (#105 & #106 Dremel) to create a craniotomy for the electrode array. The electrode was lowered onto the dura with a stereotaxic electrode positioner. With the electrode in place, a round piece of cover glass 3.0 mm in diameter (Warner Instruments) was placed over the craniotomy, and the cover glass was encircled with small pieces of gel foam. A small piece of drape was used to occlude the window while UV acrylic was applied around the edge of the glass and up to the connector. Once the electrode and connector were stable, the electrode positioner was removed. The ground/reference wire was then placed

over the area of thinned bone on the other side of the sagittal suture with a piece of gel foam and covered with UV acrylic. The mouse was then recovered while maintaining supplemental oxygen and heat.

2.3. Chronic neural interface testing with LEDs

Over subsequent weeks, we recorded neural signals from the micro-ECoG array while applying pulses of blue light through the cortical window under sedation. The mice were sedated with ketamine (75 mg/kg SC) and dexmedetomidine (25 μg/kg SC), and supplemented with oxygen and a heating pad. A Tucker-Davis Technologies system (RZ2 & PZ2) was used to sample the signals at 3 kHz and to generate LED control signals. The voltage pulses were converted to current pulses (0–1000 mA, 0.5–12 ms) with an LED driver (BuckBlock, LED dynamics). Initial experiments (figure 2 and 3) were done by simply photostimulating the entire cortical window with an LED (465 nm, RGB MC-E, Cree) positioned 20 mm away producing 0 to 0.75 mW/mm^2 (0 to 5.3 mW total applied to the window). Irradiance was found by measuring optical power (PM100D, S130C, Thor Labs) 20 mm from the LED, and the result was divided by the sensor's area. In subsequent experiments (figures 4, 5 and 6), up to 4 LEDs were focused onto the cortical surface through a microscope (MZ16F, Leica) and individually controlled by separate drivers. The optical meter was used again to measure the total power, and the area was measured with the microscope. Each LED could be focused down to a spot 150 μm in diameter at 115x magnification. The stimulus location relative to the electrode sites was recorded manually or with a camera as multiple stimulus locations were tested. Multiple stimuli were applied at each location while recording the micro-ECoG signal. Atipamezole (0.5 mg/kg SC) was given to reverse dexmedetomidine at the end of the recording session. Rectangular light pulses were generally applied, except when testing the spatio-spectral response (figure 6) in which a frequency ramped sine wave (from 0.5–200 Hz increasing at 10 $cycles/s^2$) was used.

Control experiments were conducted to verify the optogenetic origin of the observed signals (figure 2(b) and supplementary figure 2). Since ChR2/H134R is primarily excited by blue light, we used an RGB LED (RGBW MC-E Star, Cree) to apply either blue or red light to verify that only blue light generates photostimulation. We also implanted and tested wild type mice (n=2) lacking the ChR2 gene.

2.4. LASER-coupled fiber experiments

A fiber-coupled LASER system [44] was used to deliver light to known depths below the electrode array and cortical surface (figure 7). These experiments were done terminally. The procedure was similar to the cranial window implantation described above through the placement of the electrode array on the dura. The anesthesia was switched from isoflurane, which blocks neural signals, to ketamine (75 mg/kg/hr SC) and dexmedetomidine (25 μg/kg/hr SC) at least 20 minutes before beginning data acquisition. Buprenorphine was given as before (0.05 mg/kg SC). The craniotomy was left open and an optical fiber (200 μm in diameter, 0.22 NA, flat cleaved and polished, Thorlabs) was inserted into the cortex with a stereotaxic positioner which was equipped with a digital micrometer to precisely measure the depth of the fiber's tip. The fiber was advanced into the cortex 150 μm at a time, and micro-ECoG potentials were recorded in response to several stimuli at each depth. A 100

mW 473 nm LASER (Laserglow, Toronto, Canada) was used to produce photostimuli pulses 3 ms in duration and up to a power of 80 mW/mm^2 at the tip of the fiber. Irradiance was found by measuring optical power (PM100D, S130C, Thor Labs) and then dividing this value by the diameter of the fiber.

2.5. Polyimide and Parylene optical transmission

While designing electrode arrays for this study, we considered using Polyimide or Parylene C as the insulative substrate. Polyimide is an amber colored flexible insulator previously used in microelectrode arrays[45–50,4], while Parylene C is colorless polymer commonly used to coat implantable devices. We compared the transmission of blue light through 25 μm samples of each polymer into a 1% agar gel mixed in 0.9% phosphate buffered saline (PBS). The polyimide sample was prepared while fabricating arrays for another study[51]. The samples were laid along the side of a block of agar (7.5 x 40 x 40 mm). We aimed the fiber coupled LASER horizontally through the polymer samples and into the agar. The transmitted light was imaged with a digital color camera and stereoscope (DFC300 FX, MZ16 F, Leica). The images were spatially filtered (low-pass FIR, 0.01 pixels/μm corner frequency, 0.219 pixels/μm spatial sampling rate, order 50) to remove LASER speckles and isointensity contour lines were interpolated at levels relative to the maximum value when no polymer sample was present (supplementary figure 1).

2.6. In vivo and brain slice imaging

An *in vivo* image of cortical and dural blood vessels under the electrode was taken 6 weeks after implantation (figure 1(e)). We used an epifluorescence stereomicroscope (Leica MZ16 F, 546/10 nm excitation, 590 nm long pass) following tail vein injection (0.1 ml, 10 mg/ml) of rhodamine B isothiocyanate dextran (70,000 MW, R9379, Sigma-Aldrich). Rhodamine-B was chosen for minimal spectral overlap with ChR2 excitation. A video of the stimulus location was captured (figure 5(a)) by attaching a video camera to the Leica MZ16 F. Frames were captured from the video for the figure.

A fixed brain slice was imaged to locate ChR2-YFP expression. A mouse was transcardially perfused with 15 ml of PBS followed by 15 ml of 4% paraformaldehyde in PBS to fix the brain, and 500 μm thick coronal slices were cut with a vibrating microtome (Campden Instruments). YFP expression of an entire slice 1.5 mm posterior to bregma (figure 7(b)) was imaged with epifluorescence microscopy (Leica MZ16 F, 480/40 nm excitation, 510 nm long-pass emission). To achieve better resolution, a 2-photon image was taken of the cortical layers (figure 7(c)) with 890 nm excitation (Mai Tai DeepSee, Spectra Physics) and a 10x 0.5 NA Nikon objective lens.

2.7. Micro-electrocorticography signal processing

Signals were initially recorded with no digital filtering, and later processed using Matlab. The only filter applied was a 500 Hz low-pass FIR (order 25, applied forwards & backwards to preserve phase) to remove aliasing unless otherwise specified. Multiple trials were averaged to generate event related potentials and remove uncorrelated activity. The duration versus irradiance plot (figure 2(d)) was made by recording a set of event related potentials for all combinations of photostimulus durations (0.5, 1.0, 2.0 & 4.0 ms) and irradiances (20,

40, 60, 80 & 100% of 0.75 mW/mm^2), measuring the peak depolarization for a single channel, and then linearly interpolating the data with Matlab's contour function. Linear interpolation was also used to localize and pseudocolor the peak potentials of the space-time varying photostimulus (figure 5). For the space-frequency figure (figure 6), Chronux 2.1 [52] was used to calculate a spectrogram of each channel with the multi-taper method (3 tapers, time-bandwidth product 5, 1 s moving window, 50 ms step size).

3. Results

3.1. Optogenetic micro-ECoG potentials

Stimulation of the cortical surface with a blue LED (465 nm, 3 ms, 5.3 mW across the window, 0.75 mW/mm^2) in Thy1-ChR2/H134R +/− mice produced large negative micro-ECoG potentials that were readily distinguishable from background activity (figure 2(a)). These negative potentials were consistent with ChR2 stimulation as they persisted for several milliseconds after the light pulse turned off (figure 2(b), left), and blue (but not red) light evoked a response that was absent in wild type mice (figure 2(b), supplementary figure 2). ChR2 evoked potentials were highly reliable with similar amplitude potentials being produced on each trial, especially at large amplitudes (figure 2(a)). When we applied the photostimulus to the entire window, the averaged potentials were spatially uniform, and stimuli longer in duration evoked larger amplitude potentials than brief stimuli (figure 2(c)). The amplitude of the potentials depended on both the photostimulus duration and brightness (i.e. irradiance), so we systematically explored this parameter space for single pulses of light (figure 2(d)). Given a desired potential amplitude, parameters for single pulses could be selected from this graph.

Light-induced artifacts were a potential issue for this hybrid approach. While the photoelectric effect was not a major concern as the energy of a blue photon of light is below the work function of the metals used in our arrays, the Becquerel effect (a.k.a. photochemical effect) could create light-induced artifact. The Becquerel effect scales linearly with the site impedance [18], so the relatively low impedance of our micro-ECoG sites (~50 kOhms @ 1 kHz) may help keep the artifact small. We controlled for optically induced artifacts in multiple ways. Wild type mice showed no response to blue photostimuli (figure 2(b) and supplementary figure 2), while ChR2 expressing mice responded to blue but not red light. We replicated the LED setup with an array in saline. The Becquerel effect was very small at less than 10 μV for a 10 ms pulse (0.75 mW/mm^2, 465 nm) and required hundreds of trials to be resolved (supplementary figure 3). This light-induced artifact was orders of magnitude smaller than the signals observed in ChR2 mice, and the artifact was tightly time locked to the photostimulus, whereas in ChR2 mice the potentials followed the photostimulus for tens of milliseconds (figure 2(b)). The high expression level of ChR2 in the chosen transgentic mice, the extended photocurents afforded by the H134R mutation, and the broad application of light to the entire window helps explain why fairly large optogenetic signals were observed for a fairly low level of irradiance (0.75 mW/mm^2).

We investigated the ability to resolve two stimuli separated by a short interval by applying pairs of photostimuli. A second pulse 1–12 ms after the first caused an additional negative potential that could be resolved for pulse separations of 4 ms or greater (figure 3). At lower

stimulus levels, the additional potential evoked by the second pulse was similar to that of the first pulse, but at higher stimulus levels, the additional potential evoked by the second pulse was less than the first (compare rows 1 and 3 of figure 3). This describes a saturation effect. Subsequently, we investigated spatial activation and localization of neural activity.

3.2. Spatial localization

Focal photostimulation of a small cortical area (200 μm in diameter) was achieved by focusing an LED through a microscope objective (1 mW, 32 mW/mm^2, 465 nm, 20 nm FWHM). This focal stimulation evoked a spatial distribution of potentials with the largest amplitudes nearest the stimulus site (figure 4(a)). The spatial distribution of potentials changed with each new stimulus location. We tested the spatial resolution of the interface, the ability to distinguish signal originating at two locations separated by distance. Two LEDs were focused on the cortex and simultaneously applied. These two sources could be distinguished from the micro-ECoG potentials when the stimuli were greater than 1 mm apart (figure 4(c)), but the stimuli could not be distinguished when separated by smaller distances (figure 2(b)). Multiple sources were separable after averaging stimulus trials (figure 4(c)), but more sophisticated localization algorithms could also be applied [53,54].

3.3. Space-time & frequency characterization

Complex photostimuli, varying both in time and space were applied to the cortex to further assess the cortical response to stimuli at multiple locations and with varied frequency content. To demonstrate stimuli varying in both time and space, we focused a 2x2 array of blue LEDs onto the cortex. The LEDs were sequentially illuminated every 125 ms in a clockwise pattern (figure 5(a)). Each stimulus location could be spatially localized with two-dimensional interpolation from the cycle-averaged micro-ECoG recordings (figure 5).

To test the space-frequency response of the cortex, we applied a frequency-ramped sine wave photostimulus to an area of cortex 400 μm in diameter. Electrode sites nearest the stimulus location recorded a larger signal that decreased as distance and frequency increased (figure 6). Stimulation frequencies below 50 Hz generated the largest response, which corresponds to the closing time constant for ChR2/H134R of 20 ms [36]. Deactivation of the ChR2 channel due to prolonged stimulation also accounts for roughly half of the ChR2 conduction decrease over time [36], but a change of many decibels can be seen after 50 Hz. After characterizing surface stimuli varying in time, frequency, and two spatial dimensions across the cortical surface, the third spatial dimension remained. We investigated neural activity below the cortical surface using an acute preparation and an optical fiber.

3.4. Intracortical fiber stimulation

Photostimuli were applied at multiple depths below the cortical surface by advancing an optical fiber stereotaxically during an acute surgical procedure (figure 7(a)). The fiber was coupled to a 473 nm LASER [44]. Photostimulation with the optical fiber caused spatially defined potentials with the largest amplitudes observed nearest to the stimulus, similar to focal stimulation at the surface through the microscope. Multiple negative and positive potential peaks were observed at high stimulation intensities (2.5 mW, 78 mW/mm^2, 3 ms) (figure 7(d)), but only the first negative peak remained when the intensity was decreased

(0.8 mW, 25.5 mW/mm^2) (figure 7(e)). These additional peaks at high stimulus intensities could be due to cortical circuitry with synaptic transmission to and inhibitory feedback from interneurons, or these multiple peaks could be due to pyramidal neurons in deeper layers responding more slowly. Expression of ChR2/H134R-YFP was found in layers 2/3 and 5 at similar levels (figure 7 (c)). As we inserted the fiber deeper, the initial negative potential peak decreased in amplitude, but the subsequent positive peaks increased with a maximum amplitude occurring when the fiber tip was positioned 300 μm deep within the cortex. As a control for light induced-artifacts, we found that the addition of isoflurane reduced the size of the potentials, and half an hour following the end of this terminal procedure, no light-induced artifacts were measureable. Further investigation with intracortical electrode arrays and modeling of this phenomenon will be necessary, but the current data could be readily applied to validating epileptic source localization algorithms.

5. Discussion

Optogenetics is an effective approach for studying temporal and cell-type specific aspects of micro-ECoG. We found that exciting pyramidal neurons in the upper layers of the cortex causes negative micro-ECoG potentials (figures 2 & 4). This result was in accordance with Ayling et al. who also reported negative potentials when recording from the cortical surface in Thy1-ChR2 mice with silver wire electrodes [23]. Depolarization of neurons with ChR2 would be expected to create a negative potential as a net flux of cations enters the cells, leaving behind a net negative charge. Interestingly, this negative potential was less apparent when the photostimulus was deeper within the cortex (figure 7). This could be investigated with computer simulations bridging neuron models, optogenetics, and electrostatics [55], but it is an open question whether a model with multiple cell types is required to account for the multiple potential peaks observed in figure 7(d). Using this system, optogenetics could be used to determine the contribution of specific cell types to the micro-ECoG signal. Studies in mice expressing ChR2 in interneurons have reported the generation of gamma rhythms [56,57], a frequency band of great importance to the ECoG community for BCI implementation [2] and cortical mapping [58].

Optogenetic micro-ECoG has potential applications for the study of epilepsy and other diseases affecting the electrophysiology of the cortex. Localizing aberrant neural activity from EEG or ECoG recordings remains a challenging inverse problem that requires a priori assumptions to be made about the nature of the solution (see [59] for a review), and direct verification of source localization algorithm performance is difficult, requiring the researcher to cause neural activity at a known time and location [53]. Towards testing a priori assumptions about the solution, it would be desirable to be able to drive multiple and spatially diffuse neural sources. This is difficult to do electrically, but relatively simpler to do optogenetically due to the inherent parallelism of light. Stimulating multiple neural sources simultaneously was readily achievable (figure 4) and more complex photostimulation could be induced with more advanced optical hardware (e.g. spatial light modulators). Additional directions relevant to epilepsy research include optogenetically testing the effect of antiepileptic drugs on cortical excitability, studying the effect of activating specific cell types during epileptic episodes, investigating the cortical dynamics of

channelopathy mouse models, and developing closed-loop seizure detection and optogenetic stimulation protocols.

As a bidirectional neural interface, optogenetic micro-ECoG could be used in a wide set of applications and experimental approaches. Sensorimotor neuroprostheses are a potential application of our approach, but miniaturization and integration of the optical hardware would be required. Motor signals could be decoded from micro-ECoG, and information from sensors on the prosthesis could be fed back to the sensory cortex optogenetically. Feedback can also be applied more generally in closed-loop paradigms in which the photostimuli depend on recorded signals in real-time. The amount of activity at a cortical region could be regulated, effectively pacing the cortex, or virtual connections could be formed by cross-connecting recording sites and photostimulation sites. These artificial connections could be used to interact with network connectivity models of the cortex or perhaps to bridge over an infarcted region. Cerebral vascular imaging and other *in vivo* approaches add more line of investigation.

Adding *in vivo* imaging and improving the optical hardware are the next steps for development of this platform. The cranial windowing technique we adapted for this study for the purpose of photostimulation also provided excellent views of cerebral vasculature for multiple weeks (figure 1(e)). Neurovascular coupling is an obvious route for investigation. The middle cerebral artery was apparent with epifluorescence imaging, but more advanced imaging techniques such as 2-photon or optical coherence tomography would help resolve deeper vessels. More advanced optical patterning hardware would also be helpful, since we were limited to a small number of LEDs. An optical system with a spatial light modulator would greatly improve spatial photostimulation capabilities. Further development and integration of optical systems will broaden the spectrum of applications for optogenetic micro-ECoG.

Supplementary Material

Refer to Web version on PubMed Central for supplementary material.

Acknowledgments

Special thanks to Steven Skroch for insightful discussions about combining optogenetics and electrode arrays.

This work was sponsored by the Defense Advanced Research Projects Agency (DARPA) MTO under the auspices of Dr. Jack Judy through the Space and Naval Warfare Systems Center, Pacific Grant/Contract No. N66001-12-C-4025.

This work was also supported by the National Institutes of Health NIBIB grant T90 DK070079.

References

1. Penfield W, Jasper H. Epilepsy and the functional anatomy of the human brain. 1954
2. Leuthardt EC, Schalk G, Wolpaw JR, Ojemann JG, Moran DW. A brain–computer interface using electrocorticographic signals in humans. J Neural Eng. 2004; 1:63–71. [PubMed: 15876624]
3. Wilson JA, Felton EA, Garell PC, Schalk G, Williams JC. ECoG factors underlying multimodal control of a brain-computer interface. Neural Systems and Rehabilitation Engineering, IEEE Transactions on. 2006; 14:246–50.

4. Rubehn B, Bosman C, Oostenveld R, Fries P, Stieglitz T. A MEMS-based flexible multichannel ECoG-electrode array. J Neural Eng. 2009; 6:036003. [PubMed: 19436080]
5. Viventi J, Kim D-H, Vigeland L, Frechette ES, Blanco JA, Kim Y-S, Avrin AE, Tiruvadi VR, Hwang S-W, Vanleer AC, Wulsin DF, Davis K, Gelber CE, Palmer L, Van der Spiegel J, Wu J, Xiao J, Huang Y, Contreras D, Rogers JA, Litt B. Flexible, foldable, actively multiplexed, high-density electrode array for mapping brain activity in vivo. Nat Neurosci. 2011; 14:1599–605. [PubMed: 22081157]
6. Rouse AG, Williams JJ, Wheeler JJ, Moran DW. Cortical Adaptation to a Chronic Micro-Electrocorticographic Brain Computer Interface. J Neurosci. 2013; 33:1326–30. [PubMed: 23345208]
7. Otto KJ, Rousche PJ, Kipke DR. Microstimulation in auditory cortex provides a substrate for detailed behaviors. Hearing Research. 2005; 210:112–7. [PubMed: 16209915]
8. Venkatraman S, Elkabany K, Long JD, Yao Y, Carmena JM. A System for Neural Recording and Closed-Loop Intracortical Microstimulation in Awake Rodents. IEEE Transactions on Biomedical Engineering. 2009; 56:15–22. [PubMed: 19224714]
9. Boyden ES, Zhang F, Bamberg E, Nagel G, Deisseroth K. Millisecond-timescale, genetically targeted optical control of neural activity. Nat Neurosci. 2005; 8:1263–8. [PubMed: 16116447]
10. Zhang F, Wang L-P, Brauner M, Liewald JF, Kay K, Watzke N, Wood PG, Bamberg E, Nagel G, Gottschalk A, Deisseroth K. Multimodal fast optical interrogation of neural circuitry. Nature. 2007; 446:633–9. [PubMed: 17410168]
11. Chow BY, Han X, Dobry AS, Qian X, Chuong AS, Li M, Henninger MA, Belfort GM, Lin Y, Monahan PE, Boyden ES. High-performance genetically targetable optical neural silencing by light-driven proton pumps. Nature. 2010; 463:98–102. [PubMed: 20054397]
12. Gradinaru V, Thompson KR, Zhang F, Mogri M, Kay K, Schneider MB, Deisseroth K. Targeting and Readout Strategies for Fast Optical Neural Control In Vitro and In Vivo. J Neurosci. 2007; 27:14231–14238. [PubMed: 18160630]
13. Royer S, Zemelman BV, Barbic M, Losonczy A, Buzsáki G, Magee JC. Multi-array silicon probes with integrated optical fibers: light-assisted perturbation and recording of local neural circuits in the behaving animal. European J Neurosci. 2010; 31:2279–91. [PubMed: 20529127]
14. Yizhar O, Fenno LE, Prigge M, Schneider F, Davidson TJ, O'Shea DJ, Sohal VS, Goshen I, Finkelstein J, Paz JT, Deisseroth K. Neocortical excitation/inhibition balance in information processing and social dysfunction. Nature. 2011
15. Anikeeva P, Andalman AS, Witten I, Warden M, Goshen I, Grosenick L, Gunaydin LA, Frank LM, Deisseroth K. Optetrode: a multichannel readout for optogenetic control in freely moving mice. Nat Neurosci. 2012; 15:163–70. [PubMed: 22138641]
16. Wang J, Wagner F, Borton DA, Zhang J, Ozden I, Burwell RD, Nurmikko AV, van Wagenen R, Diester I, Deisseroth K. Integrated device for combined optical neuromodulation and electrical recording for chronic in vivo applications. J Neural Eng. 2012; 9:016001. [PubMed: 22156042]
17. Cardin JA, Carlén M, Meletis K, Knoblich U, Zhang F, Deisseroth K, Tsai L-H, Moore CI. Targeted optogenetic stimulation and recording of neurons in vivo using cell-type-specific expression of Channelrhodopsin-2. Nat Protocols. 2010; 5:247–54.
18. Khurram, A.; Seymour, JP. Investigation of the photoelectrochemical effect in optoelectrodes and potential uses for implantable electrode characterization*. 2013 35th Annual International Conference of the IEEE Engineering in Medicine and Biology Society (EMBC); 2013. p. 3032-5.
19. Kwon, K.; Li, W. Integrated multi-LED array with three-dimensional polymer waveguide for optogenetics 2013. IEEE 26th International Conference on Micro Electro Mechanical Systems (MEMS); 2013. p. 1017-20.
20. Forbes, Henry S. The cerebral circulation: I. observation and measurement of pial vessels. Arch Neurol Psy. 1928; 19:751–61.
21. Holtmaat A, Bonhoeffer T, Chow DK, Chuckowree J, Paola VD, Hofer SB, Hübener M, Keck T, Knott G, Lee W-CA, Mostany R, Mrsic-Flogel TD, Nedivi E, Portera-Cailliau C, Svoboda K, Trachtenberg JT, Wilbrecht L. Long-term, high-resolution imaging in the mouse neocortex through a chronic cranial window. Nature Protocols. 2009; 4:1128–44.

22. Drew PJ, Shih AY, Driscoll JD, Knutsen PM, Blinder P, Davalos D, Akassoglou K, Tsai PS, Kleinfeld D. Chronic optical access through a polished and reinforced thinned skull. Nat Meth. 2010; 7:981–4.
23. Ayling OGS, Harrison TC, Boyd JD, Goroshkov A, Murphy TH. Automated light-based mapping of motor cortex by photoactivation of channelrhodopsin-2 transgenic mice. Nat Meth. 2009; 6:219–24.
24. Aravanis AM, Wang L-P, Zhang F, Meltzer LA, Mogri MZ, Schneider MB, Deisseroth K. An optical neural interface: in vivo control of rodent motor cortex with integrated fiberoptic and optogenetic technology. Journal of Neural Engineering. 2007; 4:S143–S156. [PubMed: 17873414]
25. Yizhar O, Fenno LE, Davidson TJ, Mogri M, Deisseroth K. Optogenetics in neural systems. Neuron. 2011; 71:9–34. [PubMed: 21745635]
26. Yuen TGH, Agnew WF, Bullara LA. Tissue response to potential neuroprosthetic materials implanted subdurally. Biomaterials. 1987; 8:138–41. [PubMed: 3555632]
27. Stieglitz T, Kammer S, Koch KP, Wien S, Robitzki A. Encapsulation of flexible biomedical microimplants with parylene C. IFESS 2002. 2002; 5
28. Loeb GE, Bak MJ, Salcman M, Schmidt EM. Parylene as a Chronically Stable, Reproducible Microelectrode Insulator. IEEE Trans Biomed Eng. 1977; 24:121– 128. [PubMed: 408260]
29. Schmidt EM, Mcintosh JS, Bak MJ. Long-term implants of Parylene-C coated microelectrodes. Med Biol Eng Comput. 1988; 26:96–101. [PubMed: 3199908]
30. Rodger DC, Fong AJ, Li W, Ameri H, Ahuja AK, Gutierrez C, Lavrov I, Zhong H, Menon PR, Meng E, Burdick JW, Roy RR, Edgerton VR, Weiland JD, Humayun MS, Tai Y-C. Flexible parylene-based multielectrode array technology for high-density neural stimulation and recording. Sensor Actuat B-Chem. 2008; 132:449–60.
31. Ledochowitsch, P.; Olivero, E.; Blanche, T.; Maharbiz, MM. A transparent μECoG array for simultaneous recording and optogenetic stimulation. 2011 Annual International Conference of the IEEE Engineering in Medicine and Biology Society, EMBC (IEEE); 2011. p. 2937-40.
32. Wilks SJ, Richner TJ, Brodnick SK, Kipke DR, Williams JC, Otto KJ. Voltage Biasing, Cyclic Voltammetry, & Electrical Impedance Spectroscopy for Neural Interfaces. J Vis Exp. 2012
33. Arenkiel BR, Peca J, Davison IG, Feliciano C, Deisseroth K, Augustine GJ, Ehlers MD, Feng G. In Vivo Light-Induced Activation of Neural Circuitry in Transgenic Mice Expressing Channelrhodopsin-2. Neuron. 2007; 54:205–18. [PubMed: 17442243]
34. Zhao S, Ting JT, Atallah HE, Qiu L, Tan J, Gloss B, Augustine GJ, Deisseroth K, Luo M, Graybiel AM, Feng G. Cell type-specific channelrhodopsin-2 transgenic mice for optogenetic dissection of neural circuitry function. Nat Meth. 2011; 8:745–52.
35. Nagel G, Brauner M, Liewald JF, Adeishvili N, Bamberg E, Gottschalk A. Light Activation of Channelrhodopsin-2 in Excitable Cells of Caenorhabditis elegans Triggers Rapid Behavioral Responses. Curr Biol. 2005; 15:2279–84. [PubMed: 16360690]
36. Lin JY, Lin MZ, Steinbach P, Tsien RY. Characterization of Engineered Channelrhodopsin Variants with Improved Properties and Kinetics. Biophys J. 2009; 96:1803–14. [PubMed: 19254539]
37. Mattis J, Tye KM, Ferenczi EA, Ramakrishnan C, O'Shea DJ, Prakash R, Gunaydin LA, Hyun M, Fenno LE, Gradinaru V, Yizhar O, Deisseroth K. Principles for applying optogenetic tools derived from direct comparative analysis of microbial opsins. Nat Meth. 2012; 9:159–72.
38. LEVASSEUR JE, WEI EP, RAPER AJ, KONTOS HA, PATTERSON JL. Detailed Description of a Cranial Window Technique for Acute and Chronic Experiments. Stroke. 1975; 6:308–17. [PubMed: 1154467]
39. Morii S, Ngai AC, Winn HR. Reactivity of Rat Pial Arterioles and Venules to Adenosine and Carbon Dioxide: With Detailed Description of the Closed Cranial Window Technique in Rats. J Cerebr Blood F Met. 1986; 6:34–41.
40. Trachtenberg JT, Chen BE, Knott GW, Feng G, Sanes JR, Welker E, Svoboda K. Long-term in vivo imaging of experience-dependent synaptic plasticity in adult cortex. Nature. 2002; 420:788–94. [PubMed: 12490942]
41. Mostany R, Portera-Cailliau C. A Craniotomy Surgery Procedure for Chronic Brain Imaging. J Vis Exp. 2008

42. Yoder EJ, Kleinfeld D. Cortical imaging through the intact mouse skull using two-photon excitation laser scanning microscopy. Microsc Res Techniq. 2002; 56:304–5.
43. Schendel AA, Thongpang S, Brodnick SK, Richner TJ, Lindevig BDB, Krugner-Higby L, Williams JC. A cranial window imaging method for monitoring vascular growth around chronically implanted micro-ECoG devices. Journal of Neuroscience Methods. 2013; 218:121–30. [PubMed: 23769960]
44. Pashaie R, Falk R. Single Optical Fiber Probe for Fluorescence Detection and Optogenetic Stimulation. IEEE Trans Biomed Eng. 2013; 60:268– 280. [PubMed: 23060317]
45. Stieglitz T, Beutel H, Meyer JU. A flexible, light-weight multichannel sieve electrode with integrated cables for interfacing regenerating peripheral nerves. Sensor Actuat A-Phys. 1997; 60:240–3.
46. Grumet AE, Wyatt JL Jr, Rizzo JF III. Multi-electrode stimulation and recording in the isolated retina. Journal of Neuroscience Methods. 2000; 101:31–42. [PubMed: 10967359]
47. Rousche PJ, Pellinen DS, Pivin DP, Williams JC, Vetter RJ, Kipke DR. Flexible polyimide-based intracortical electrode arrays with bioactive capability. IEEE Trans Biomed Eng. 2001; 48:361–71. [PubMed: 11327505]
48. Stieglitz T. Flexible biomedical microdevices with double-sided electrode arrangements for neural applications. Sensors and Actuators A: Physical. 2001; 90:203–11.
49. Takahashi H, Ejiri T, Nakao M, Nakamura N, Kaga K, Herve T. Microelectrode array on folding polyimide ribbon for epidural mapping of functional evoked potentials. IEEE Trans Biomed Eng. 2003; 50:510–6. [PubMed: 12723063]
50. Hollenberg BA, Richards CD, Richards R, Bahr DF, Rector DM. A MEMS fabricated flexible electrode array for recording surface field potentials. J Neurosci Met. 2006; 153:147–53.
51. Thongpang S, Richner TJ, Brodnick SK, Schendel A, Kim J, Wilson J, Hippensteel J, Krugner-Higby L, Moran D, Ahmed AS, Williams J. A micro-electrocorticography platform and deployment strategies for chronic BCI applications. Clin EEG Neurosci. 2011; 42:259. [PubMed: 22208124]
52. Mitra, P.; Bokil, H. Observed brain dynamics. New York, New York, USA: Oxford University Press, New York, New York, USA; 2008.
53. Van Veen BD, Van Drongelen W, Yuchtman M, Suzuki A. Localization of brain electrical activity via linearly constrained minimum variance spatial filtering. IEEE Trans Biomed Eng. 1997; 44:867–80. [PubMed: 9282479]
54. Brunner P, Ritaccio AL, Lynch TM, Emrich JF, Wilson JA, Williams JC, Aarnoutse EJ, Ramsey NF, Leuthardt EC, Bischof H, Schalk G. A practical procedure for real-time functional mapping of eloquent cortex using electrocorticographic signals in humans. Epilepsy & Behavior. 2009; 15:278–86. [PubMed: 19366638]
55. Foutz TJ, Arlow RL, McIntyre CC. Theoretical principles underlying optical stimulation of a channelrhodopsin-2 positive pyramidal neuron. J Neurophysiol. 2012; 107:3235–45. [PubMed: 22442566]
56. Cardin JA, Carlén M, Meletis K, Knoblich U, Zhang F, Deisseroth K, Tsai L-H, Moore CI. Driving fast-spiking cells induces gamma rhythm and controls sensory responses. Nature. 2009; 459:663–7. [PubMed: 19396156]
57. Sohal VS, Zhang F, Yizhar O, Deisseroth K. Parvalbumin neurons and gamma rhythms enhance cortical circuit performance. Nature. 2009; 459:698–702. [PubMed: 19396159]
58. Crone N, Miglioretti D, Gordon B, Lesser R. Functional mapping of human sensorimotor cortex with electrocorticographic spectral analysis. II Event-related synchronization in the gamma band. Brain. 1998; 121:2301–15. [PubMed: 9874481]
59. Kaiboriboon K, Lüders HO, Hamaneh M, Turnbull J, Lhatoo SD. EEG source imaging in epilepsy—practicalities and pitfalls. Nat Rev Neurol. 2012; 8:498–507. [PubMed: 22868868]

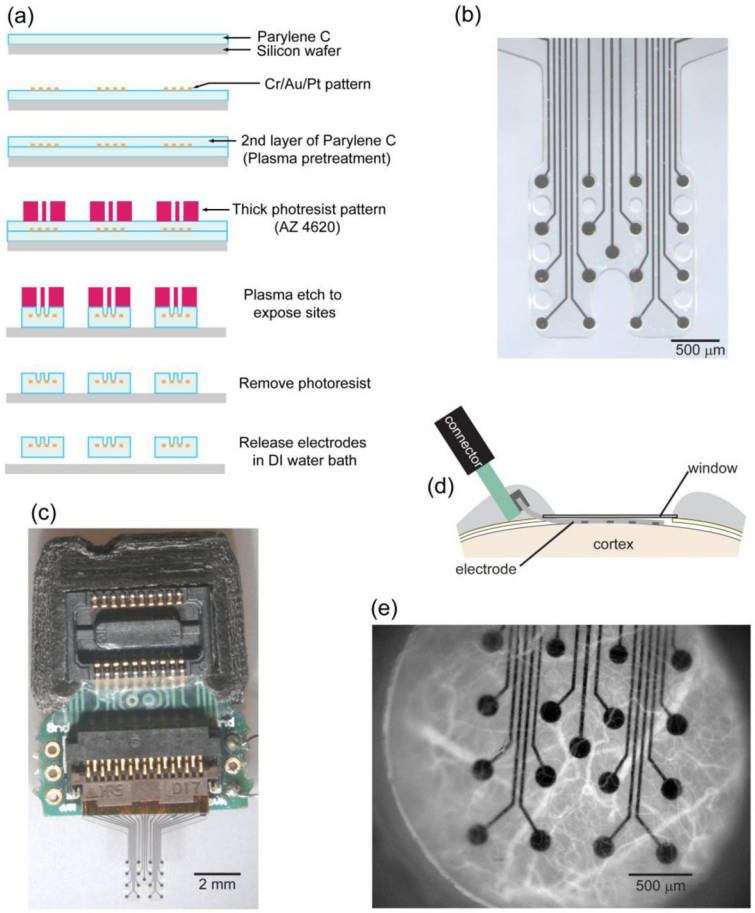

Figure 1.

Micro-ECoG array fabricated on a transparent substrate and chronically implanted under a cranial window. (a) The photolithography process involved a lift-off method to pattern metal layers onto a Parylene C coated wafer, deposition of an additional layer of Parylene, and then exposure of the electrode sites with plasma etching. (b) A micro-ECoG electrode array with platinum electrode sites patterned on Parylene C. Electrode sites 150 μm in diameter are arranged in a 4x4 grid with 500 μm between sites. (c) The electrode array was assembled with a custom printed circuit board to route traces from the FPC connector to a zero insertion force connector. The array was implanted under a cranial window in mice as illustrated in panel (d). (e) Blood vessels, labeled with rhodamine-B dextran, were visible through the cranial window and electrode for several weeks following implantation.

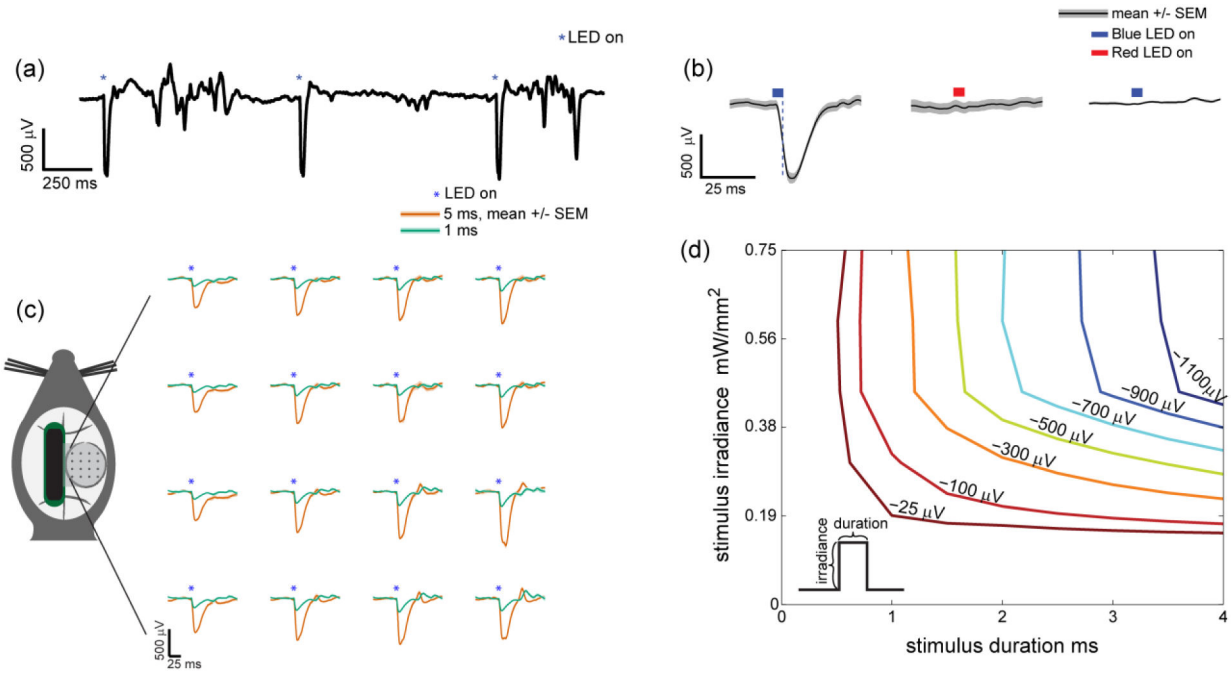

Figure 2.

Optogenetically evoked micro-ECoG potentials. (a) An unfiltered micro-ECoG signal shows large negative potentials associated with every photostimulus * (465 nm, 3 ms, 0.75 mW/mm^2, 5.3 mW applied to entire window). (b) Wild type mice did not show any response to stimulation with blue light photostimulus - (465 nm, 0.75 mW/mm^2), while ChR2 positive mice were responsive to blue - (465 nm, 0.75 mW/mm^2) but not red - (625 nm, 0.81 mW/mm^2) photostimuli. A single channel is shown with 50 trials averaged for each condition. Control figures with all 16 channels can be found in supplementary figure 2. Trial-averaged evoked potentials are mapped according to channel location on the array (1 or 5 ms, 465 nm, 0.75 mW/mm^2, 5.3 mW total across the window). Longer stimuli evoked larger negative potentials. These potentials were spatially uniform with the entire window illuminated. 10 trials were averaged for each condition. (d) The amplitude of optogenetically evoked potential depended on the duration and irradiance (i.e. brightness) of the photostimulus. The stimulus duration and irradiance parameter space was systematically explored to generate a 2D interpolated contour plot.

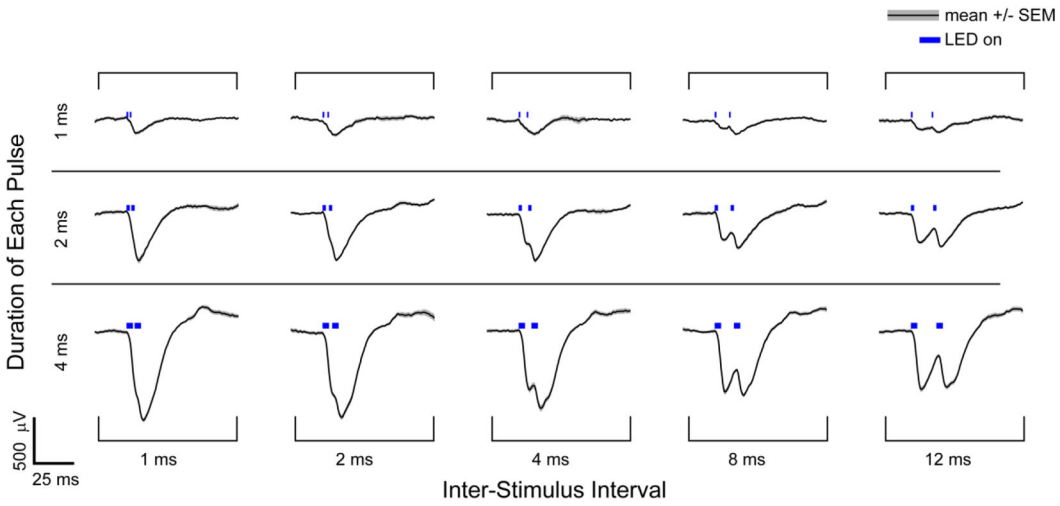

Figure 3.

Optogenetically evoked micro-ECoG potentials in response to pairs of light pulses. Averaged potentials for a single channel are shown in response to pairs of photostimuli applied at 0.75 mW/mm^2. The duration of each pulse and the inter-stimulus interval was varied. Pairs of brief stimuli (1 ms) caused negative potentials that superimposed linearly, while longer photostimuli (4 ms) did not evoke a linear response as the second peak was not twice as large as the first. Photostimuli spaced by more than 2 ms could be readily distinguished, but photostimuli seperated by less than 1 ms appeared as a single event based on the recorded signals. Between 13 and 28 trials were averaged for each condition.

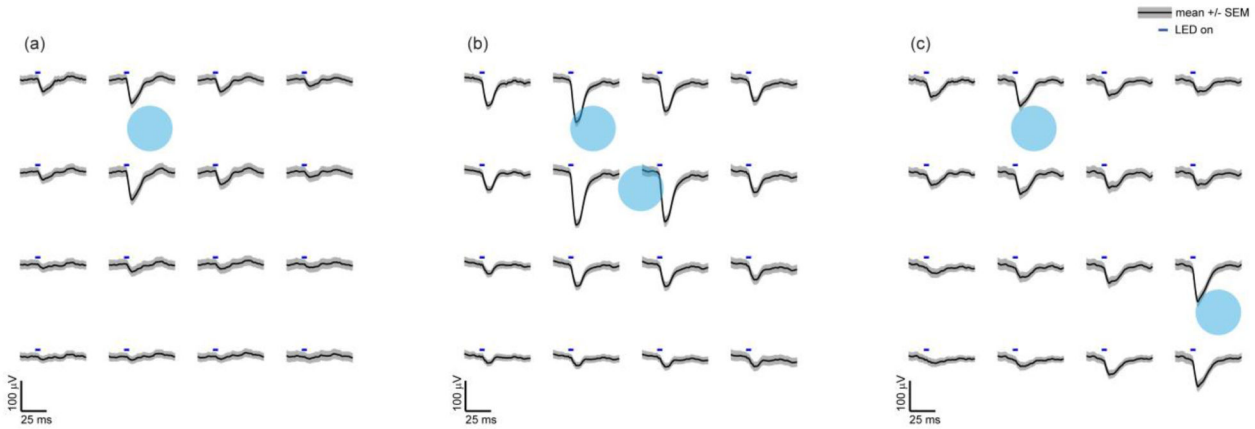

Figure 4.

Spatially mapped micro-ECoG potentials in response to focally applied optogenetic stimuli. One or two focal photostimuli ● were applied repeatedly to the cortical surface using an objective lens. The photostimuli were 200 µm in diameter, for 5 ms in duration - and 1 mW in power (32 mW/mm^2). (**a**) The amplitude of the evoked micro-ECoG potentials was greatest nearest the stimulus location. Surrounding electrode sites had similar but smaller amplitude waveforms with minimal phase delay suggesting electrostatic volume conduction. (**b**,**c**) Stimultaneously applied focal photostimuli evoke spatially separable potentials at distances greater than twice the electrode spacing (**c**), but at closer electrode spacings the evoked potentials were less separable. 90 trials were averaged for each.

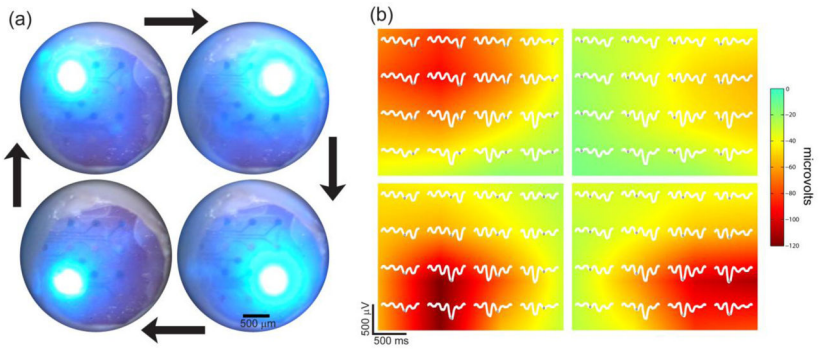

Figure 5.

Spatiotemporal photostimulation and localization. (a) Photostimuli were applied at four locations in sequence. Four LEDs were focused on the cortex and illuminated in a clockwise sequence at 2 cycles per second. (b) The corresponding cycle averaged micro-ECoG potentials (100 cycles averaged) are plotted in white for each position. The peak potential for each stimulus location is marked ○, and these values were pseudocolored using linear interpolation. Spatially localized potentials were observed for each stimulus location. Potentials were bandpass filtered from 5 to 500 Hz.

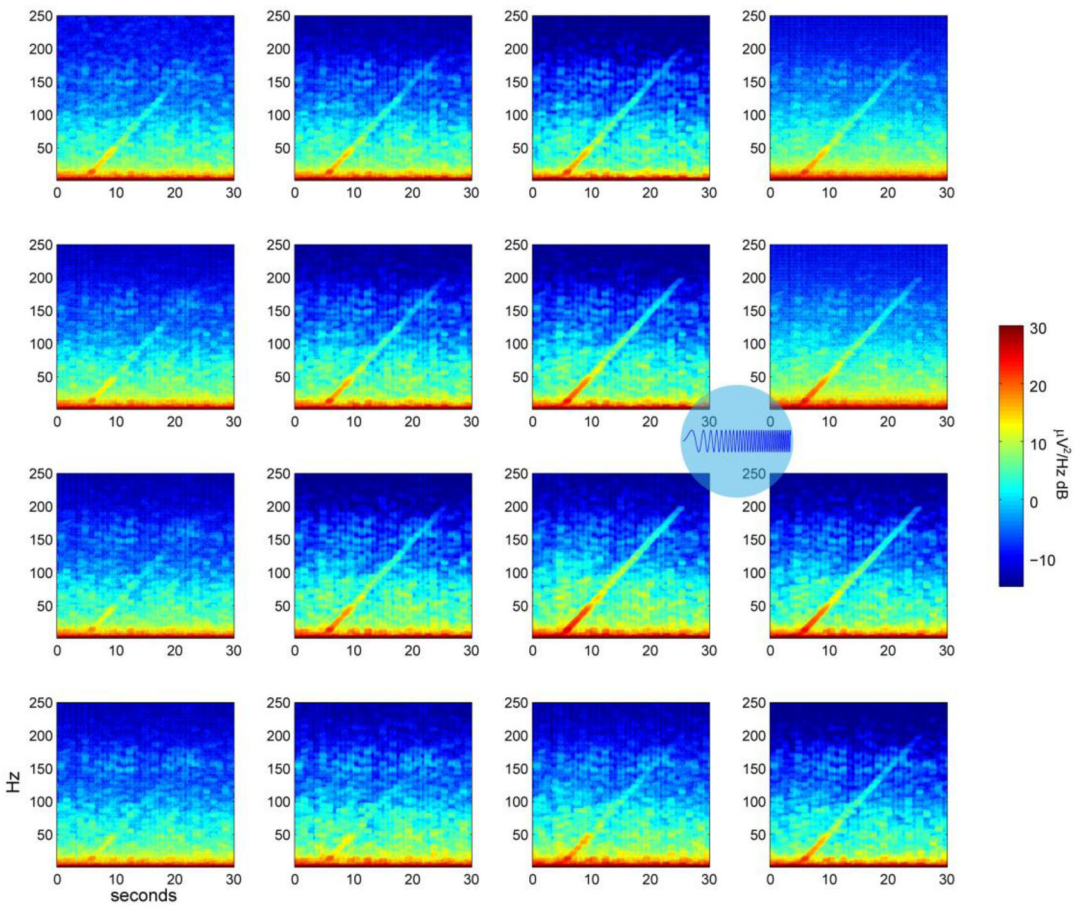

Figure 6.

The spatio-spectral cortical response. A frequency-ramped photostimulus was applied to an area 500 μm in diameter between the electrode sites ●. Spectrograms of the signals at each micro-ECoG electrode site show that the cortical response decreases as distance and frequency increase. 5 trials were averaged.

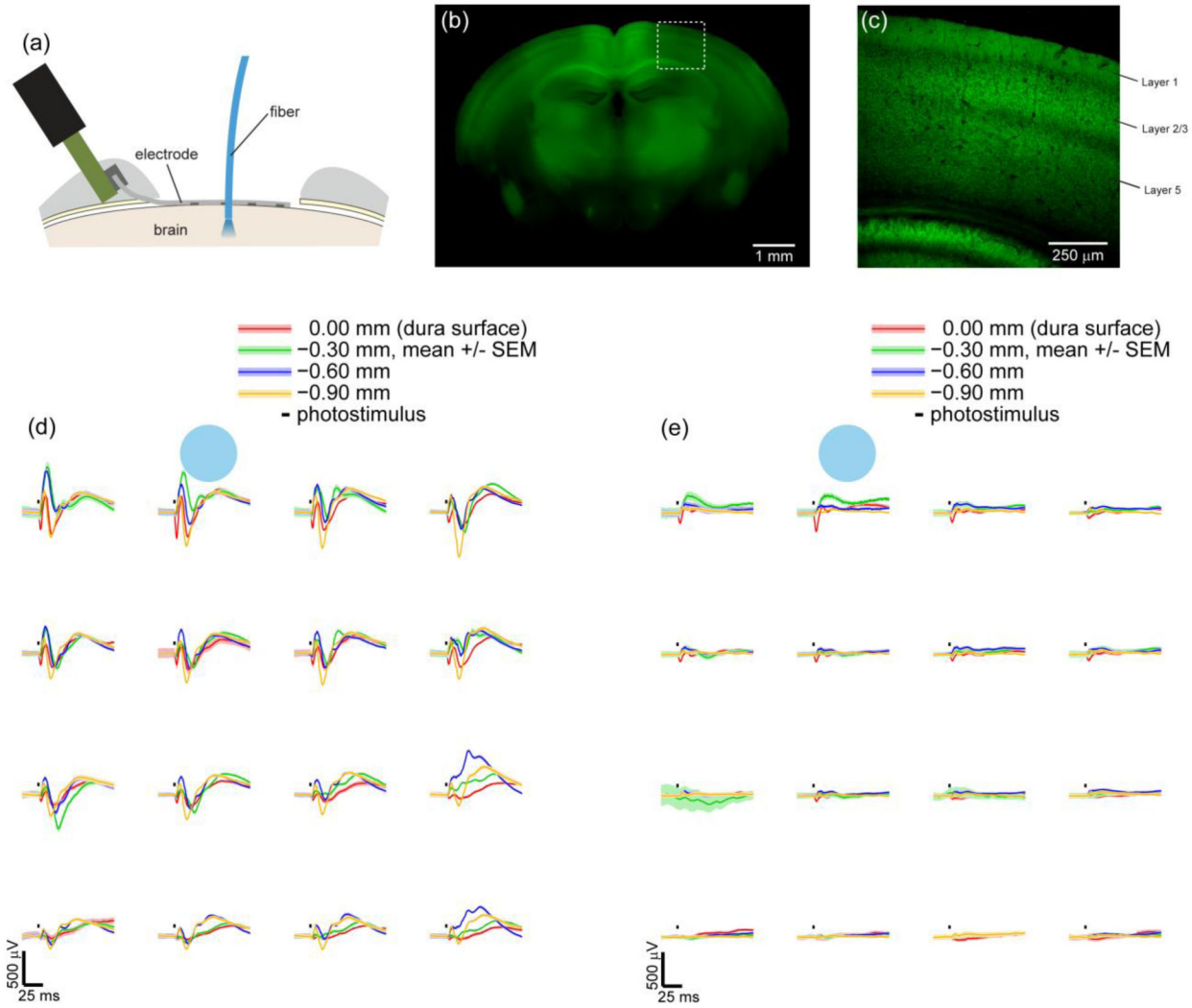

Figure 7.

Optogenetically evoked micro-ECoG potentials in response to photostimuli applied intracortically with a fiber-coupled LASER or at depths below the cortical surface with a LASER coupled fiber. (a) A cross section diagram of a micro-ECoG electrode array on the dura and a fiber inserted into the cortex. Expression of ChR2/H134R-YFP under the Thy1 promoter in found in a subset of cortical layers. (b) Epifluorescence of an entire coronal slice 1.5 mm posterior to bregma shows expression in the cortex, hipocampus, and thalamus. Greater cortical expression is found medially, but the implanted region (0.5 to 3.5 mm lateral) has more uniform expression. (c) A two-photon image of the outlined region in (b) shows expression in cortical layers 2/3 and 5. Layer 1 also has expression but no cell bodies, suggesting expression in apical dendrites. (d,e) Averaged potentials recorded from the micro-ECoG array in response to photostimuli - (3 ms, 473 nm) applied next to the array ● at multiple depths within the cortex. Photostimulus power was 2.5 mW (78 mW/mm^2) in (d) and 0.8 mW (25.5 mW/mm^2) in (e). Stronger photostimuli (d) caused potentials with multiple negative and positive peaks, while weaker photostimuli (e) evoked only an initial negative peak. These subsequent peaks followed several miliseconds after the photostimulus

ceased. Similar to figure 4, the amplitude of the micro-ECoG potentials (d,e) were spatially related to the stimulus location. 50 trials were averaged for each condition in (d) and (e).